

Physics-based evaluation of the drapability of textile composite reinforcements.

Renzi Bai, Bo Chen, Julien Colmars, Philippe Boisse*

Univ Lyon, INSA Lyon, CNRS, LaMCoS, UMR5259, 69621, Villeurbanne, France

Abstract.

The drapability of a textile composite reinforcement is its capability to be formed on a double curved shape without wrinkling. This is an important property of a textile reinforcement when it is used to manufacture a preform in liquid composite molding processes. The analysis of the deformation modes and the form of the internal virtual works during draping of a fibrous reinforcement leads to define a physics-based Drapability Ratio determined by the in-plane shear stiffness and the bending stiffness of the textile reinforcement. This Drapability Ratio can be used to identify the reinforcement that can be draped for a given geometry. Square box forming and cylindrical forming carried out for a set of textile reinforcements under the same conditions show the relevance of this Drapability Ratio.

Keywords: A. Fabrics/textiles, D. Mechanical testing, E. Preform, E. Forming

1. Introduction

Liquid Composites Molding (LCM) process [1,2] is a technology used to manufacture composite parts in the aeronautical and automotive industries [3-6]. In these processes, the first step is a forming of a textile reinforcement. It is followed by an injection of the resin on the obtained preform. The present study considers continuous fiber textile reinforcements that provide the best mechanical properties to composites. This forming process, often called draping, is delicate when the geometry of the part is complex. Many studies have had, and currently have, the objective of analyzing this stage [7-9]. Numerical simulation codes for this draping step have been developed and are making steady progress [10-19].

When manufacturing a composite, it is necessary that the draping of the textile reinforcement is carried out without defect [20 -23]. In particular, wrinkling, which is a major flaw during draping, should be avoided [24-29]. There are several factors that can contribute to the development of wrinkles when forming a fabric. The geometry of the tools (mold, punch, die), the presence or absence of blank holders, the forming velocity, in particular play an important role. Wrinkles occur when draping over the surface of the tools leads to deformations where the minimum energy solutions contain folding. Besides these process parameters, the properties of the textile reinforcement, which are linked to its internal structure, have a major contribution to the development of wrinkles. This aptitude is a material property of the fabric called drapability.

* Corresponding author: philippe.boisse@insa-lyon.fr

In the field of composite manufacturing, the classical definition of the drapability of a textile reinforcement is its capability to be formed on a double curved shape without wrinkling [30]. Other points are important for a successful forming, in particular the adequate direction of the fibers, the fiber volume fraction in the final composite part. Only the ability to be draped without wrinkling is considered in this study. A textile reinforcement can or cannot be used to make complex double-curvature geometries depending on its drapability which is an important property for a textile composite reinforcement. However, this drapability of the fabric is not sufficient to rule on the possibility of wrinkle-free draping of a given forming process because factors external to the textile reinforcements have roles of primary importance. To determine the possibility of a draping without wrinkles, a numerical simulation relevant to the description of the wrinkles should be performed. Nevertheless, drapability is an essential property for the producer of a textile composite reinforcement and for the manufacturer of textile preforms to know if strongly double curved geometries can be considered for a given fabric.

The study of drapability has mainly been carried out by using an experimental device called Drape Meter [31-39]. In a classical Drape Meter, a circular sample of radius R_2 is draped under its own weight onto a support plate of smaller radius R_1 . (Fig. 1). The vertical projection of the contour of the draped sample defines an area A_r (Fig. 1b). By noting A_1 the area of the support disk and A_2 the area of the disk of the initial textile sample, the Drape Coefficient DC is obtained by $DC=(A_r-A_1)/(A_2-A_1)$.

The lower the DC value, the greater the drapability of the fabric studied. This method allows to estimate the drapability of textiles or at least to compare them. However, this approach has several drawbacks. The method does not measure a physical quantity and the drape coefficient DC is dependent on the test device. The test lacks repeatability may be unstable, and the draped geometry can evolve over time [34,36,38]. Some alternative devices dedicated to drapability measurement have been developed. In particular, the Drapetest drapability tester is presented in [30] that uses the principle of pushing a hemispherical reference body against a clamped textile sample to forcibly drape the textile into that shape.

The objective of this paper is to propose a simple method to evaluate the drapability of a textile composite reinforcement from its mechanical characteristics, without using a drape meter. For this purpose, an analysis of the different energies of deformation during a draping process is made. The square box forming test, known to be a complex shape to drape, was chosen to demonstrate the relevance of the approach.

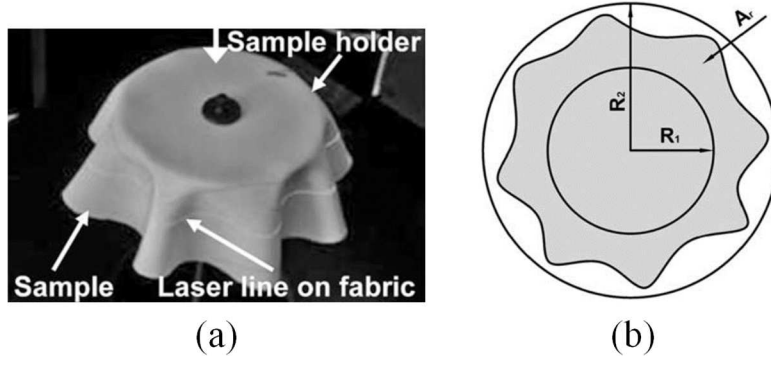


Fig. 1. (a) Drape meter. (b) Projection of the draped fabric sample [37]

2. Deformation modes and stiffnesses of a textile reinforcement during draping.

2.1. Shell approach for textile composite reinforcement

The virtual work theorem is considered for a textile reinforcement during a forming process. For any virtual displacement equal to zero on the boundary with prescribed displacements, it can be written

$$\delta W_{ext} - \delta W_{int} - \delta W_{acc} = 0 \quad (1)$$

Here, δW_{ext} , δW_{int} , δW_{acc} , are the virtual works of external, internal and acceleration quantities.

A shell approach can be used because the thickness of the fabric is small compared to its in-plane dimensions (Fig. 2) and the internal virtual work is the sum of the virtual works of tension $\delta W_{tension}$, in-plane shear δW_{shear} and bending $\delta W_{bending}$.

$$\delta W_{int} = \delta W_{tension} + \delta W_{shear} + \delta W_{bending} \quad (2)$$

$$\text{with } \delta W_{tension} = \int_A (\delta \epsilon_{11} N_{11} + \delta \epsilon_{22} N_{22}) dA \quad (3)$$

$$\delta W_{shear} = \int_A \delta \epsilon_{12} N_{12} dA \quad (4)$$

$$\delta W_{bending} = \int_A (\delta \chi_{11} M_{11} + \delta \chi_{22} M_{22} + \delta \chi_{12} M_{12}) dA \quad (5)$$

Here $\delta \epsilon_{11}$, $\delta \epsilon_{22}$ are the virtual strains in the warp and weft directions, $\delta \epsilon_{12}$ is the virtual in-plane shear strain, $\delta \chi_{11}$, $\delta \chi_{22}$, $\delta \chi_{12}$ are the virtual curvatures. N_{11} , N_{22} , N_{12} are the stress resultants and M_{11} , M_{22} , M_{12} are the stress moments (or stress couples) with:

$$N_{\alpha\beta} = \int_{-\frac{h}{2}}^{\frac{h}{2}} \sigma_{\alpha\beta} dz \quad M_{\alpha\beta} = \int_{-\frac{h}{2}}^{\frac{h}{2}} z \sigma_{\alpha\beta} dz \quad (6)$$

The indices α , β belong to the set (1, 2), $\sigma_{\alpha\beta}$ are the components of the Cauchy stress, A is the midsurface of the shell, h is its thickness.

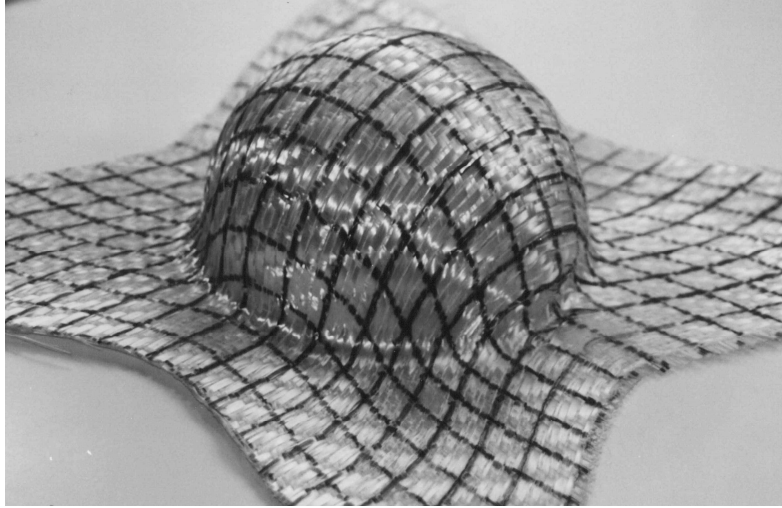


Fig. 2. Draping of a woven reinforcement on a double-curved surface.

The development of wrinkles during draping depends on the solutions given by the virtual work theorem (Eq. 1) taking into account the specific forms of the internal forces in the case of a textile reinforcement (Eq. 2 to 5), the material properties of the fabric, and the boundary conditions [40].

The study and modeling of the mechanical behavior linking the interior loads $N_{\alpha\beta}, M_{\alpha\beta}$ to the deformations $\varepsilon_{\alpha\beta}, \chi_{\alpha\beta}$ has been the subject of numerous works in the case of textile composite reinforcements. Most of these works make the simplifying assumption that these mechanical behaviors are decoupled, i.e. that the tensile behavior is given by $N_{\alpha\beta}(\varepsilon_{\alpha\beta})$ and the bending behavior by $M_{\alpha\beta}(\chi_{\alpha\beta})$ (α, β equal to 1 or 2, no sum). This assumption is adopted in the proposed approach. In addition, the mechanical behavior is assumed to be elastic. It has been shown that elastic behavior is satisfactory for modeling forming processes as long as the loading is monotonic (no unloading) which is generally the case [41]. As a consequence the tensile behavior is given by :

$$N_{11} = C_{T1}\varepsilon_{11} \quad N_{22} = C_{T2}\varepsilon_{22} \quad (7)$$

where C_{T1} and C_{T2} are the tensile stiffnesses of the fabric in the warp and weft directions.

By noting γ the shear angle, i.e. the change in angle between the warp and weft direction ($\gamma = 2\varepsilon_{12}$), the in-plane shear behavior is in the form:

$$N_{12} = C_S\gamma \quad (8)$$

where C_S is the in-plane shear stiffness. The bending behavior is given by:

$$M_{11} = C_{B1}\chi_{11} \quad M_{22} = C_{B2}\chi_{22} \quad (9)$$

where C_{B1} and C_{B2} are the bending stiffnesses of the fabric in the warp and weft directions.

The internal virtual work $\delta\chi_{12}M_{12}$ coming from twisting curvature (Eq. 5) is neglected because the total bending stiffness of the reinforcement is mainly due to the warp and weft yarns bending stiffness.

The above equations are based on the warp and weft directions of continuous fiber woven reinforcements or the two yarn directions of Non-Crimp Fabric (NCF). These are the materials considered in this work. A triaxial NCF and an isotropic sheet are also analyzed for information. They require another form of the virtual work equations. These two materials are not intended to be draped.

2.2. Influence of the different stiffnesses on wrinkling

2.2.1. Tensions

When forming some materials, especially metals, the strains can be large [42,43]. The present study focuses on textile composite reinforcements consisting of continuous yarns in the warp and weft directions which are very stiff and quasi-inextensible. The warp and weft yarns govern the deformation of the textile reinforcement, but the draping on a double curved shape is not achieved by extension of the yarns. Tension loads in the yarns (Eq. 3) can prevent the formation of wrinkles especially by the use of blank holders. However, these are devices and forces external to the material.

2.2.2. In-plane shear

Because the yarns of textile composite reinforcements are almost inextensible, forming on a double-curved surface is achieved by in-plane shear deformations (or shear angles) as shown in Fig. 2 for a hemispherical surface. These in-plane shear angles are therefore an important mode of deformation for the draping of textile reinforcements. Measuring and modeling of in-plane shear behavior has given rise to numerous studies [44-51]. The in-plane shear stiffness should be as low as possible to enable shear angles as large as needed to drape a given shape. If this stiffness is higher, it can lead to wrinkling during draping. These wrinkles have out-of-plane geometries that decrease the shear angles and thus the corresponding deformation energy. All other properties being equal, the higher the in-plane shear stiffness, the lower the drapability of the textile reinforcement. Apart from the drapability, the shear stiffness can bring some advantages, e.g. ease of handling.

2.2.3. Bending

The bending behavior of textile reinforcements is strongly influenced by their fibrous composition. The possible relative slippage of the fibers leads to a bending stiffness much lower than that of a continuous material. The relations resulting from the classical plate theories which

provide the bending stiffness from the tension stiffness and the thickness are not valid. Due to the low bending stiffness, membrane type models (neglecting the bending stiffness) have been proposed [52-58]. Nevertheless, it has been shown that the bending stiffness, although low, conditions the onset and development of wrinkles [59-61] and thus plays an important role in the drapability of textile reinforcements. The formation of wrinkles causes curvatures and provides bending deformation energy. The bending stiffness counteracts the wrinkle formation and therefore favors draping without wrinkles. All other properties being equal, the higher the bending stiffness, the higher the drapability of the textile reinforcement. The increase in bending stiffness can have disadvantages such as increased forces during forming. For a given manufacturing process, this aspect should be analyzed.

2.3. Drapability Ratio

In plane shear and bending stiffnesses influence the drapability of a textile reinforcement in opposite ways. On the one hand, the in-plane shear stiffness should be as low as possible to easily drape a given shape, on the other hand, the bending stiffness counteracts the wrinkle formation. The tensile characteristics do not influence the drapability because the yarns of composite reinforcements are almost inextensible. The proposed Drapability Ratio (DR) is defined from the in-plane shear and bending stiffness:

$$DR = \frac{C_S}{C_B} \quad (\text{mm}^{-2}) \quad (10)$$

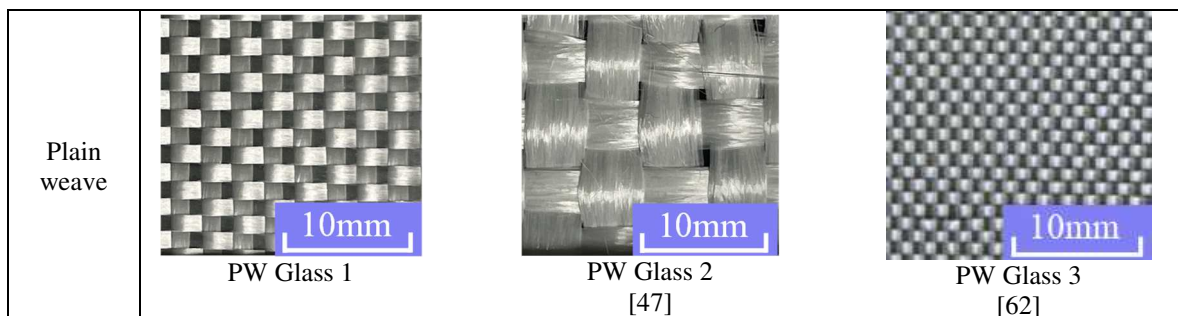
If the shear stiffness C_S is expressed in N mm^{-1} and the bending stiffness C_B in N mm then the Drapability Ratio is given in mm^{-2} . A large part of the studied textile reinforcements is balanced and therefore have the same stiffnesses in the warp and weft direction. For unbalanced fabrics, C_B is the average of the bending stiffnesses in the warp and weft direction.

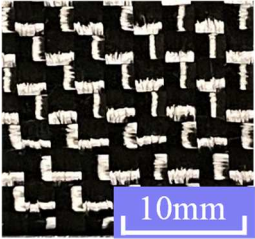
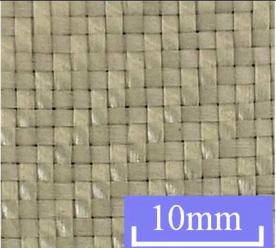
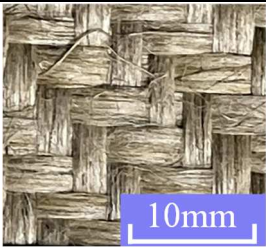
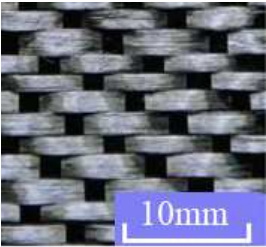
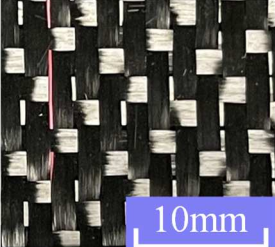
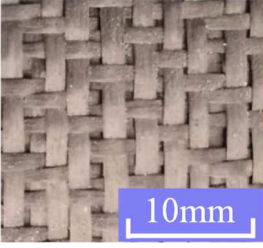
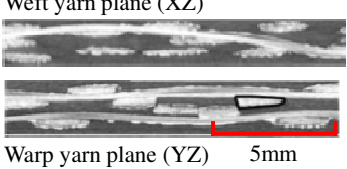
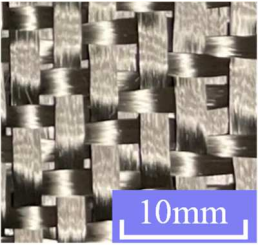
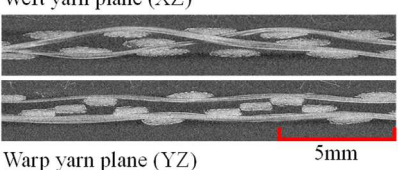
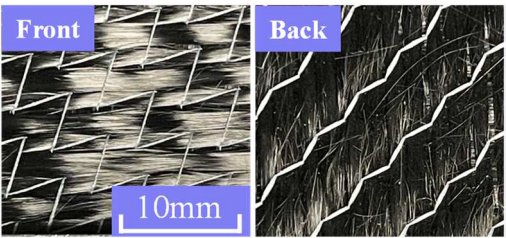
3. Measurement of shear and bending stiffnesses and determination of Drapability Ratios

3.1. Materials

The textile reinforcements whose drapability is analyzed in this paper are shown in Table 1. Their main properties are given in Table 2. In the case of interlocks G1151 and G1100, they are made up of 3 yarns in each direction linked by weaving.

Table 1. Studied textile reinforcements.



	 <p>PW Carbon 1 [63]</p>
Twill weave	  <p>TW Galss TW Flax</p>
Satin weave	  <p>SAT Carbon 1 SAT Carbon 2 [62]</p>
Interlock	  <p>G1151[®] [64]</p>   <p>G1100[®]</p>
NCF	 <p>NCF Biax</p>

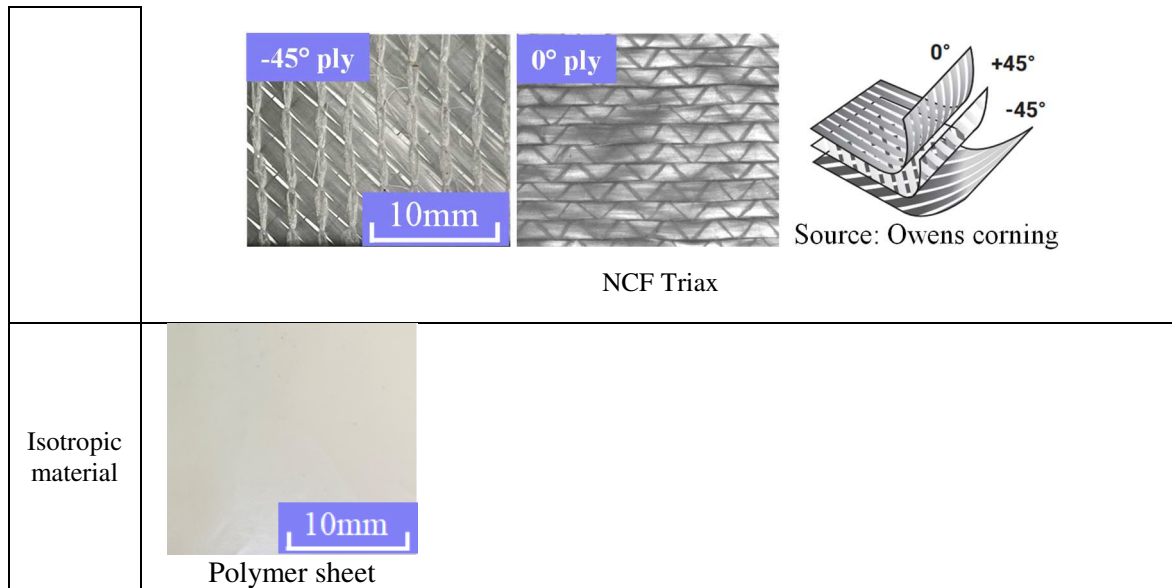


Table 2. Properties of the studied materials

Type of fabric	Plain weave				Twill weave	
Name of fabric	PW Glass 1	PW Glass 2	PW Glass 3	PW Carbon 1	TW Glass	TW Flax
Thickness (mm)	0.34	1.2	0.12	0.8	0.3	1.1
Fiber Type	Glass	Glass/PP	Glass	Carbon	Glass	Flax
Areal density (g m^{-2})	347	745	160	675	418	329
Number of warp yarns per cm	4.1	1.93	11.8	5	6.6	3.6
Number of weft yarns per cm	6.6	1.93	10.7	5	6.6	3.6

Type of fabric	Satin weave		Interlock		NCF	
Name of fabric	SAT Carbon 1	SAT Carbon 2	Hexcel G1151 [®]	Hexcel G1100 [®]	NCF Biax	NCF Triax
Thickness(mm)	0.3	0.4	1.3	1.04	0.5	1.1
Fiber Type	Carbon	Carbon	Carbon	Carbon	Carbon	Glass
Areal density (g m^{-2})	290	234	630	600	312	1133
Number of warp yarns per cm	6.5	5	7.5	7.5	5	+45°: 5 -45°: 5
Number of weft yarns per cm	6.5	5	7.4	7.4	5	0°: 4 (yarns/cm)

3.2. In-plane shear stiffness

The in-plane shear behavior of the textile reinforcement presented in Table. 1 is analyzed by bias extension tests [44-51, 65-68]. The bias extension test and the picture frame test are the two main experiments developed for the analysis of the in-plane shear behavior of textile reinforcements. The bias extension test consists of a tensile test on a specimen whose yarns are initially oriented at 45° (Fig. 3). The displacement of the tensile machine grips leads to an in-plane shearing of the specimen in the central area C, under the condition that the warp and weft

yarns rotate without slippage (trellising). The shear angle in zone B is half that in zone C and zone A does not deform. The bias extension test is easy to implement. In addition, the yarns have at least one free end which avoids the parasitic tensions that can be present in the picture frame test [69]. On the other hand, the assumption of a relative non-slippage of the warp and weft yarns is generally verified only up to a limit angle depending on the material [49]. In this test the shear angle γ is measured either directly by an optical measurement or calculated from the elongation of the specimen. The tensile force F imposed by the machine on the specimen is related to the shear force N_{12} often noted F_{sh} [48,69]:

$$N_{12}(\gamma) = F_{sh}(\gamma) = \frac{F D}{\ell(2D - \ell)\cos\gamma} \left(\cos\frac{\gamma}{2} - \sin\frac{\gamma}{2} \right) - \frac{\ell \cos\frac{\gamma}{2}}{(2D - \ell)\cos\gamma} F_{sh}\left(\frac{\gamma}{2}\right) \quad (11)$$

The initial lengths L and D and the initial width ℓ of the specimen are defined in Fig.3a. The in-plane shear curve measured for fabric G1151[®] (manufactured by Hexcel) is displayed in Fig. 4. The shear stiffness increases with the shear angle. This is due to the progressive lateral contacts between the yarns [64, 69]. The in-plane shear curve is not linear. However, to make the Drapability Ratio simple and easy to determine, the in-plane shear stiffness C_s in Eq. (10) is obtained from the shear force for an angle of 40° . This angle is large but can be reached easily when forming. The values of the plane shear stiffness C_s for the textile reinforcements presented in Table 1 are given in Table 3. (The choice of the in-plane shear stiffness value for an angle of 40° is discussed in section 6.3)

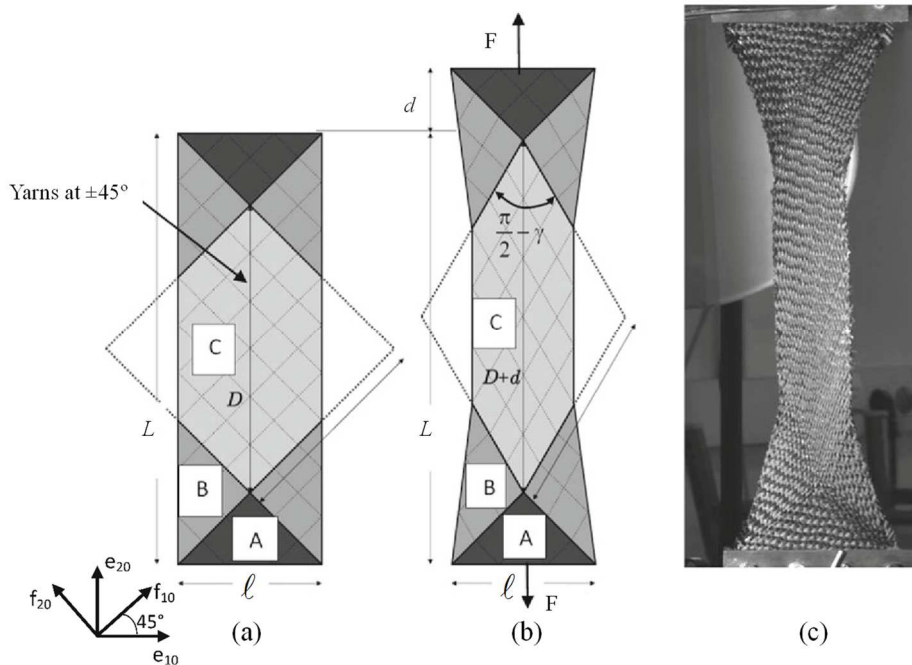


Fig. 3. Bias extension test. (a) Initial geometry. (b) Deformed shape, (c) Experiments

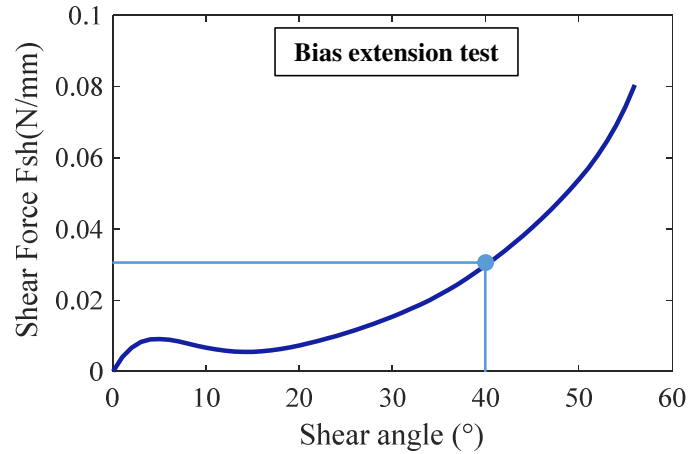


Fig. 4. In-plane shear curve of G1151®

In the case of triaxial NCF, the picture frame test is preferred. The $\pm 45^\circ$ directions were clamped to the frame and the third fiber direction was perpendicular to the traction direction in order to avoid any fiber tension. This test gives an in-plane shear stiffness equal to 3.8 N mm^{-1} . The in-plane shear stiffness of the isotropic PVC sheet was obtained by performing a tensile test which leads to a Young's modulus $E = 822 \text{ MPa}$ therefore, taking $\nu = 0.5$ for a polymer, to a shear modulus $G = E/2(1 + \nu) = 274 \text{ MPa}$. The shear stiffness $C_s = Gh/2$ is equal to 68 N mm^{-1} . This value is obtained in the context of small strains and gives an order of magnitude in the present drapability study.

3.3. Bending stiffness

The bending stiffness of textile reinforcements can be determined by several experimental methods. The Kawabata bending test imposes a curvature to the specimen by rotation of the two ends [70-72]. In this paper, the bending stiffnesses are measured by a cantilever bending test. The textile specimen is subjected to its own weight with one end clamped (Fig. 5).

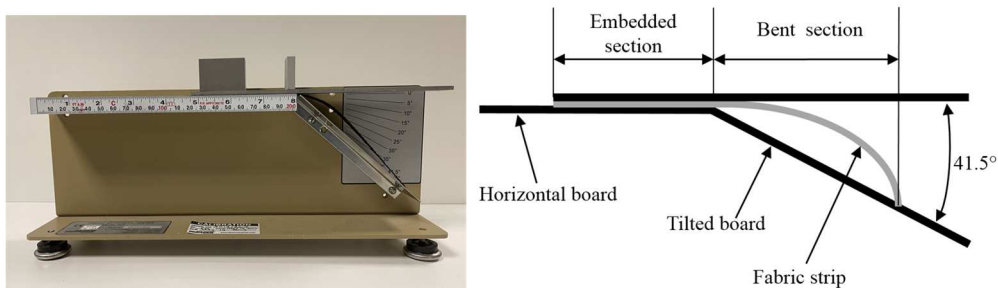


Fig. 5. Peirce's Cantilever bending test [73, 77]

From the bending moment created by the gravity loads, the measurement of the curvature of the deformed midline determines the bending behavior $M(\chi)$ (M is the bending moment and χ is the

curvature) for all curvatures between a zero value at the free end and the curvature at the clamped edge [78]. The obtained bending curve $M(\chi)$ is not always linear but the non-linearities are generally limited.

In the Pierce's test, the specimen is advanced progressively until its end comes into contact with a plane inclined at 41.5° (Fig. 5) [73-77]. Assuming that the bending behavior is linear and thus that $M = C_b \chi$, the measurement of the length ℓ of the bent part of the sample (Fig.5) gives an approximation of the bending stiffness C_B :

$$C_B = \frac{\ell^3 w}{8} \quad (12)$$

Here w is the weight of the fabric per unit area. The bending stiffnesses determined by this approach for the textile reinforcements shown Table 1 are given in Table 3.

Table 3. In-plane shear stiffness, bending stiffness and Drapability Ratio of the analyzed textile reinforcements.

Material	In-plane shear stiffness C_s (N mm ⁻¹)	Bending stiffness C_B (N mm)	Drapability Ratio DR (mm ⁻²)
PW Glass 1	0.0097	0.21	0.046
PW Glass 2	0.091	2.73	0.033
PW Glass 3	0.026	0.10	0.26
PW Carbon 1	0.22	1.38	0.16
TW Glass	0.030	0.47	0.064
TW Flax	0.056	2.57	0.022
SAT Carbon 1	0.069	3.42	0.020
SAT Carbon 2	0.040	3.05	0.013
G1151	0.041	4.52	0.0091
G1100	0.026	3.36	0.0077
NCF Biax	0.010	0.95	0.011
NCF Triax	3.8	2.17	1.75
Polymer isotropic sheet	68	0.74	92.6

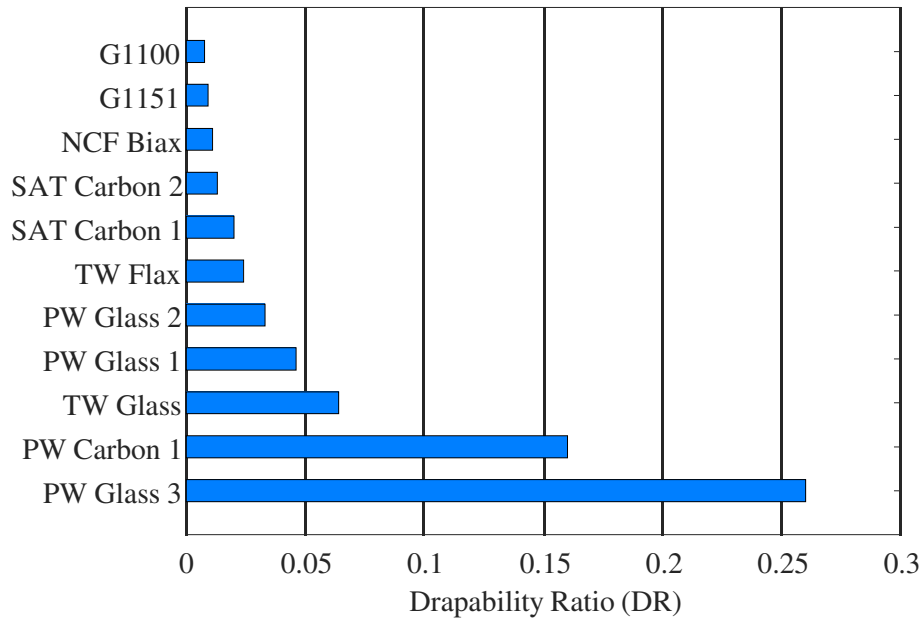


Fig.6. Drapability Ratios for the analyzed textile reinforcements

The Drapability Ratios of the different textile reinforcements obtained from Eq. (10) are given in Table 3 and Fig. 6.

The in-plane shear and bending stiffness of the various reinforcements and thus their Drapability Ratio depend on the internal structure of the textile reinforcements. Some weaves (satin, interlock) lead to lower (better) DR than others (plain weave). This point is discussed in section 6.3.

The Drapability Ratio of the triaxial NCF and of the isotropic sheet are respectively 1.75 mm^{-2} and 92.6 mm^{-2} . These two values are large. They correspond to materials that are not intended to be draped.

4. Forming tests

4.1 Square box forming

The objective of these forming experiments is to analyze the draping behavior of the tested textile reinforcements and to see if the proposed draping ratio is a relevant indicator for the development of wrinkles. The considered wrinkles are undulations out of the plane of the fabric. Although the square box is a basic geometry, it is a shape that is quite difficult to drape with continuous reinforcement textiles. Due to the quasi-inextensibility of the fibers, large shear angles are required which often leads to wrinkling. The square box forming processes presented in scientific papers generally show significant wrinkling [62,63,79-81].

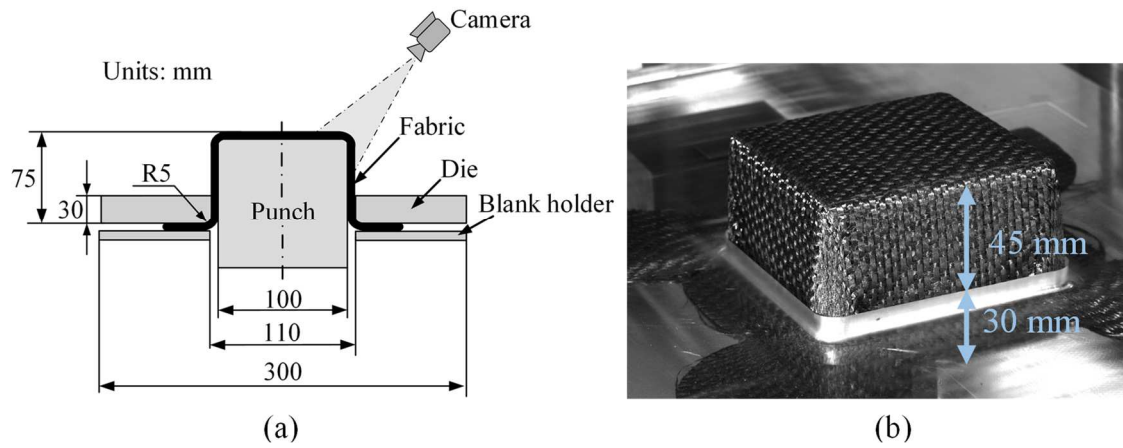
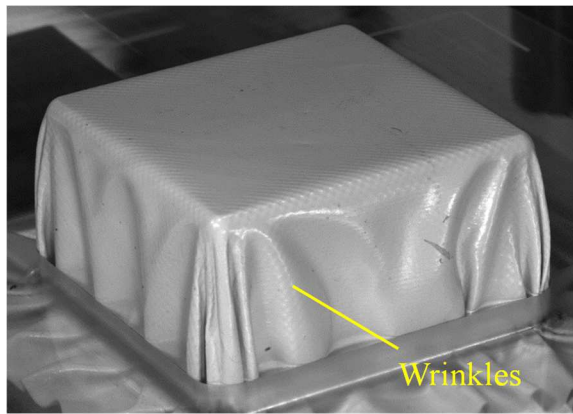
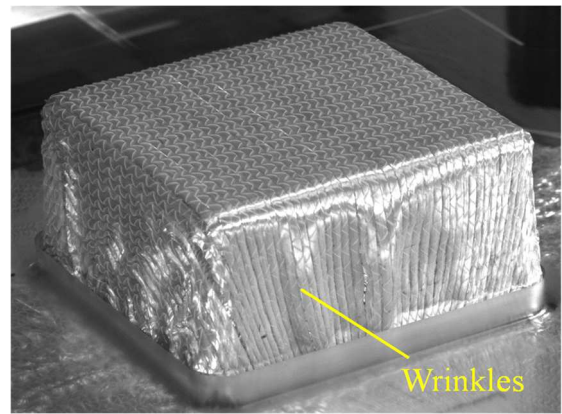


Fig. 7. Square box forming experiments (a) Geometry of the test. (b) Forming depth

Fig. 7 shows a diagram of the square box forming experiments. The depth/width ratio is equal to 0.75 which is significant, and it is the same for all the tested textile reinforcements. Fig. 7b shows that the forming depth is 75 mm, of which 30 mm is the thickness of the transparent die and 45 mm corresponds to the visible part. Figures 8 and 9 show the geometry achieved after forming of the different textile reinforcements. To measure the shear angles, pictures are captured with a camera in the resolution of 4827 x 3248 pixels. The images are zoomed in to measure the shear angle by manually tracking the warp and weft yarn.



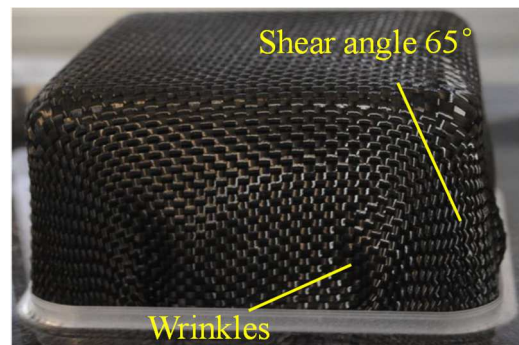
(a) Polymer isotropic sheet, DR = 92.6



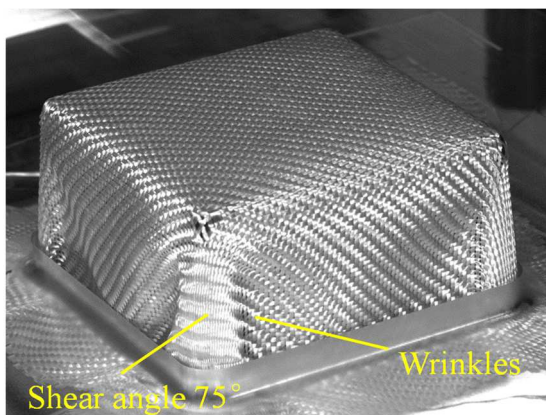
(b) NCF Triax, DR = 1.75



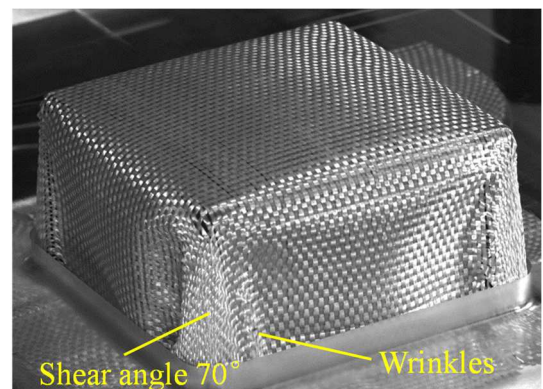
(c) PW Glass 3, DR = 0.26 [62]



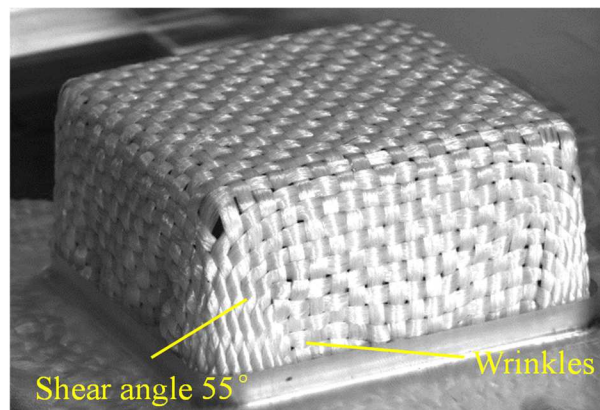
(d) PW Carbon 1, DR = 0.16 [63]



(e) TW Glass, DR = 0.064

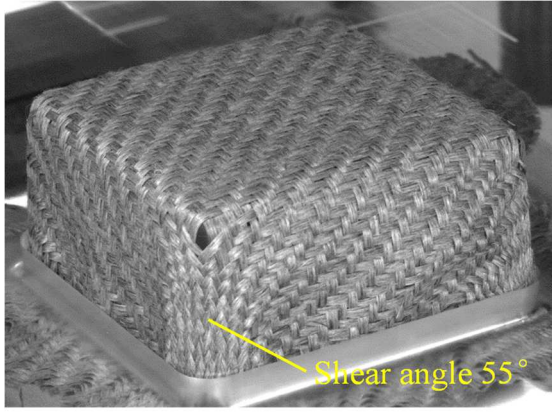


(f) PW Glass 1, DR = 0.046

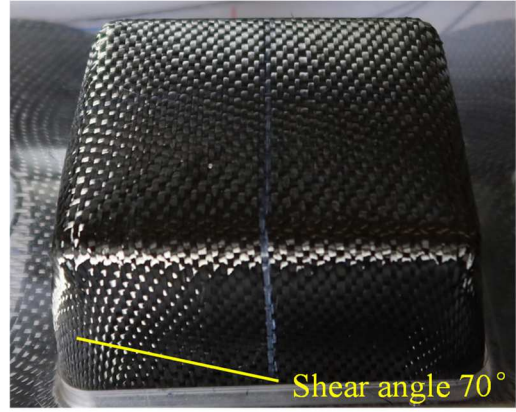


(g) PW Glass 2, DR = 0.033

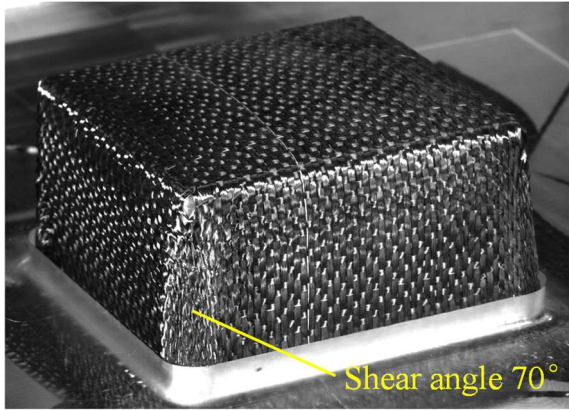
Fig. 8. Square box forming leading to wrinkling.



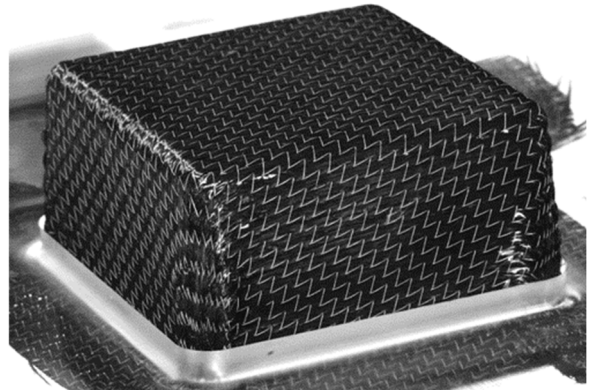
(a) TW Flax, DR = 0.022



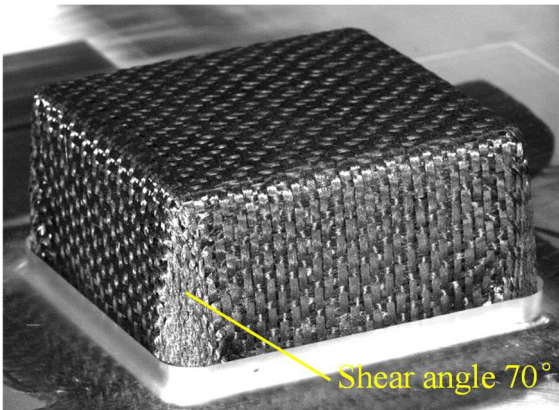
(b) Satin Carbon 1, DR = 0.020 [62]



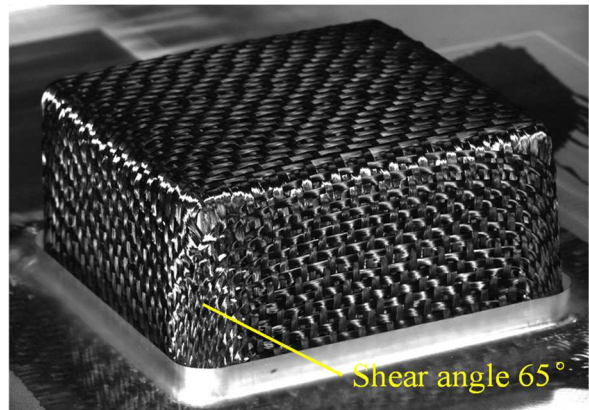
(c) Satin Carbon 2, DR = 0.013



(d) NCF Biax, DR = 0.011



(e) G1151, DR = 0.0091



(f) G1100, DR = 0.0077

Fig. 9. Square box forming without wrinkling.

The forming of the textile reinforcements shown in Fig. 8 all lead to wrinkling. These are the seven reinforcements with the highest Drapability Ratio. Moreover, the magnitude of wrinkling shows the same trend as the Drapability Ratio. The isotropic sheet and the triaxial NCF show the most severe wrinkling, while the glass plain weave 2 shows very moderate wrinkling. In Fig. 9, the forming of the six textile reinforcements is achieved without wrinkling. The Drapability Ratios of these fabrics have the smallest values. Fig. 10 shows the relationship between the Drapability Ratio and wrinkling development. There is a clear connection between the two.

The Drapability Ratio allows to classify the textile reinforcements with regard to drapability. If a forming process has been done without wrinkles for a given textile reinforcement, this forming, under the same conditions, can be done without wrinkles for all the textile reinforcements whose Drapability Ratio is lower. On the other hand, if the forming process of a textile reinforcement leads to wrinkling, all textile reinforcements with a higher Drapability Ratio will lead to wrinkling and cannot be used for this process.

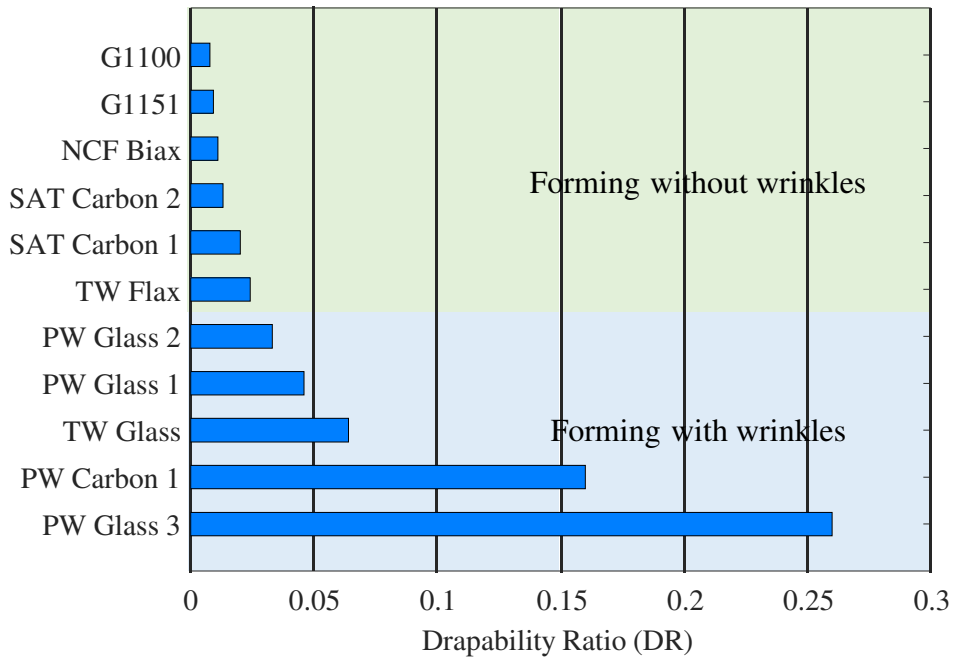


Fig. 10. Relationship between Drapability Ratio (DR) and wrinkles formation in the square box forming

4.2. Forming on a cylinder

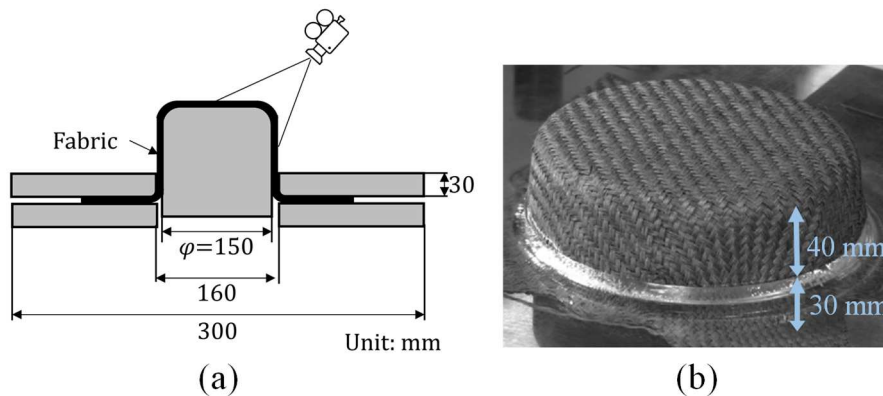


Fig.11. Cylinder forming experiments (a) Geometry of the test. (b) Forming depth.

In order to confirm the results obtained by forming on a square box, forming processes with a cylindrical punch are carried out (Fig.11). This geometry is also strongly double curved and wrinkles can develop during forming.

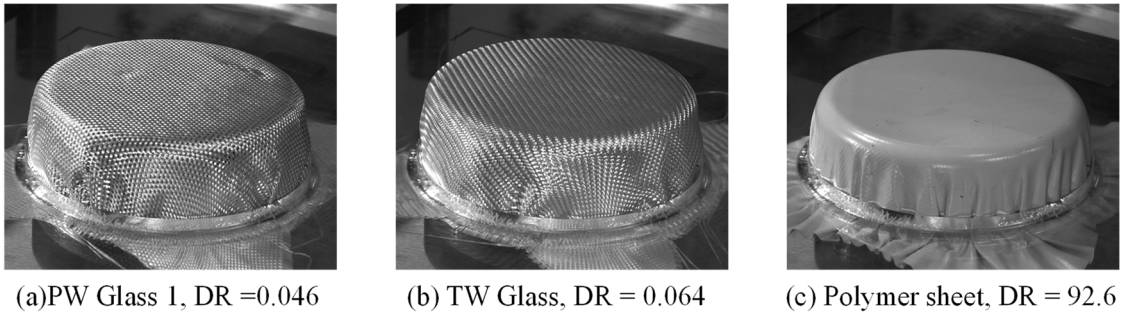


Fig.12. Cylinder forming leading to wrinkling.

Fig. 12. shows cylindrical forming that lead to wrinkling. The materials are those with the highest Drapability Ratios.

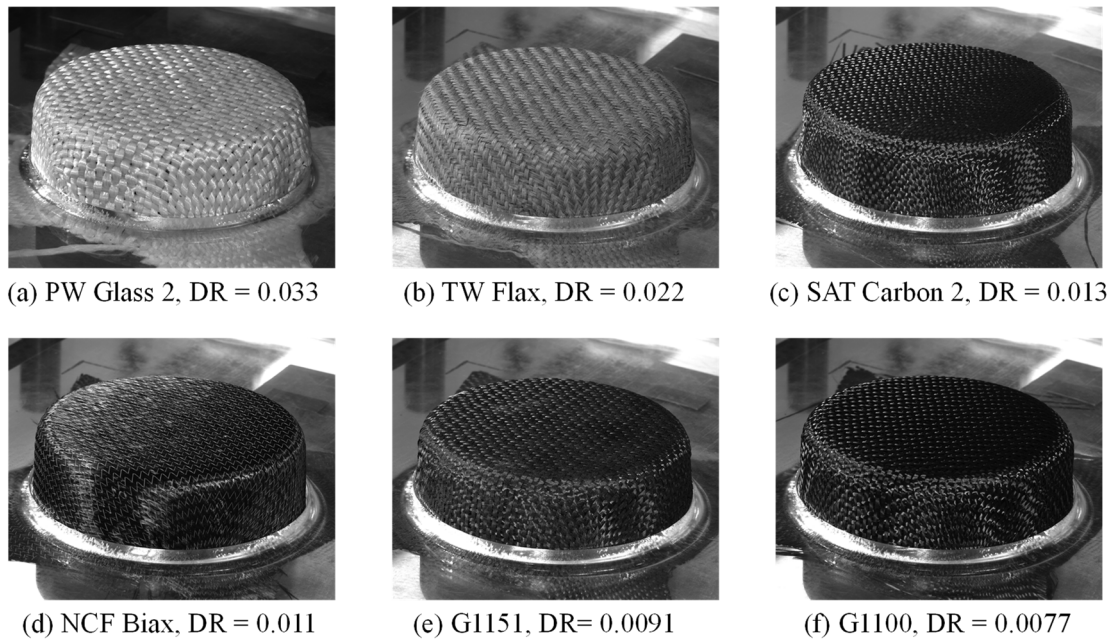


Fig.13. Cylinder forming with no wrinkle.

Fig. 13 shows draped fabrics obtained by cylindrical forming which do not show any wrinkle. The deformed fabrics do not exhibit any wrinkle although optical effects linked to the woven structure of the reinforcements could lead one to believe the contrary. Fig. 14 allows, by top view, to verify the absence of wrinkles for the reinforcements G1151 and G1100.

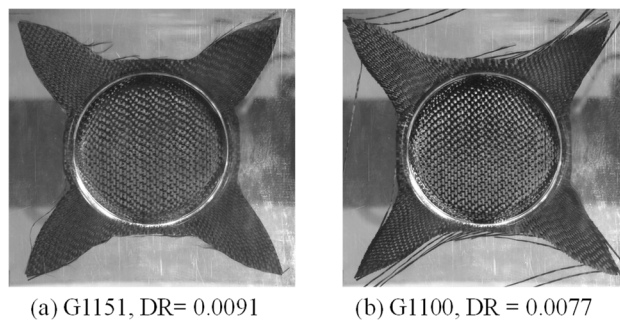


Fig. 14. Forming on a cylinder of revolution. Top view.

Forming on a revolution cylinder confirms the results obtained by draping on a square box. Textile reinforcements with low Drapability Ratio can be draped without wrinkles while those with high Drapability Ratio lead to wrinkles. The relationship between Drapability Ratio (DR) and wrinkles formation given in Fig. 10 are valid for this second process. There is, however, a nuance. The draping of the plain weave glass 2 fabric (DR = 0.033) on the square box leads to moderate wrinkling (Fig. 8g), while the forming on a cylinder is done without wrinkling (Fig. 13a). In both cases the process is at the limit of wrinkle onset, but forming on a square box is somewhat more difficult than forming on a cylinder.

5. Forming simulations

Resultant stress shell finite elements were developed from the virtual membrane and bending works given in Eq. (3) to (5) [11, 82, 83]. In this approach, the virtual works of tension (Eq. 3) and bending (Eq. 5) are calculated independently (decoupled). In addition, in-plane shear and bending stiffnesses analyzed in this study are explicitly used. The objective of this section is to show that the forming simulation results are also consistent with the Drapability Ratios of the different textile reinforcements. The materials input parameters adopted for the forming simulations are given in Table 4. Fig. 15. shows the deformed geometries obtained by the simulation of a square box forming carried out under the same conditions as those of the tests of section 4.1. (depth/width ratio equal to 0.75). The forming simulation leads to wrinkling for the two reinforcements with a high Drapability Ratio (PW Carbon 1, DR = 0.16, PW Glass 1, DR = 0.046) and no wrinkling for the textile reinforcements with a low Drapability Ratio (G1151, DR = 0.0091, G1100, DR = 0.0077). Other simulation results leading to wrinkles (PW Glass 3, DR = 0.26) and no wrinkles (SAT Carbon 1, DR = 0.020) can also be found in [62].

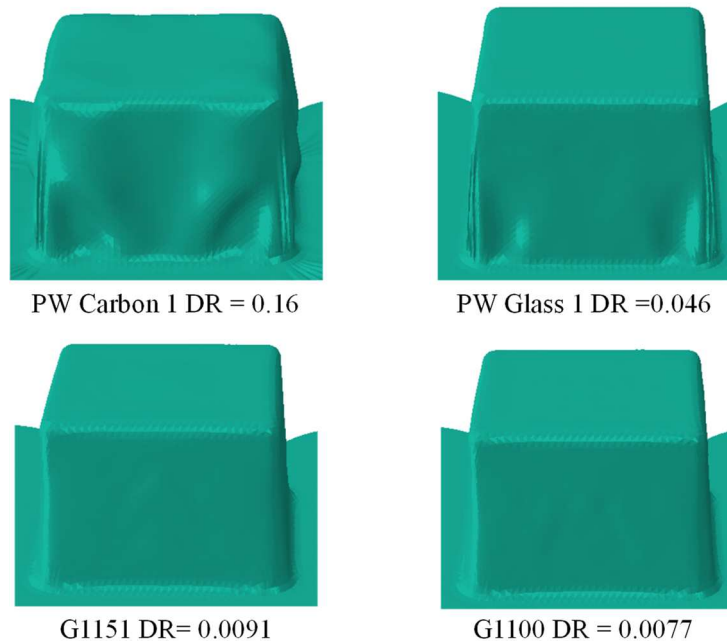


Fig. 15. Square box forming simulations

Table 4. Input parameters adopted for the forming simulations

Mechanical properties	G1100	G1151	PW Glass 1	PW Carbon 1
In plane shear $dN_{12} = C_s d\gamma$	$C_s = 0.026 \text{ N mm}^{-1}$	$C_s = 0.041 \text{ N mm}^{-1}$	$C_s = 0.0097 \text{ N mm}^{-1}$	$C_s = 0.22 \text{ N mm}^{-1}$
Out of plane bending $dM_{11} = C_{B1} d\chi_{11}$	$C_{B1} = 3.36 \text{ N mm}$	$C_{B1} = 4.52 \text{ N mm}$	$C_{B1} = 0.21 \text{ N mm}$	$C_{B1} = 1.38 \text{ N mm}$
$dM_{22} = C_{B2} d\chi_{22}$	$C_{B2} = 3.36 \text{ N mm}$	$C_{B2} = 4.52 \text{ N mm}$	$C_{B2} = 0.21 \text{ N mm}$	$C_{B2} = 1.38 \text{ N mm}$
Tensile stiffness $dN_{11} = C_{T1} d\varepsilon_{11}$	$C_{T1} = 17000 \text{ N mm}^{-1}$	$C_{T1} = 21500 \text{ N mm}^{-1}$	$C_{T1} = 1150 \text{ N mm}^{-1}$	$C_{T1} = 4600 \text{ N mm}^{-1}$
$dN_{22} = C_{T2} d\varepsilon_{22}$	$C_{T2} = 17000 \text{ N mm}^{-1}$	$C_{T2} = 21500 \text{ N mm}^{-1}$	$C_{T2} = 1150 \text{ N mm}^{-1}$	$C_{T2} = 4600 \text{ N mm}^{-1}$
Coulomb friction coefficient				
Ply to ply	0.21			
Ply to mold	0.23			

6. Discussion

6.1. Tensile deformations

The continuous fiber textile reinforcements that are used as composite reinforcements and that are the ones considered in the present study, are made of yarns very stiff in tension and close to inextensibility. For this reason, in-plane shear deformations are essential to achieve double-curved geometry. In the case of lower tensile stiffness, e.g. for knitted reinforcements [85] or stretch-broken fibers [86-88], significant in-plane elongations are possible and shaping on a complex surface is greatly facilitated. In these cases, the Drapability Ratio as defined in Eq. (10) is not relevant. It is restricted to the case of classical composite reinforcements with yarns in the warp and weft directions made of continuous fibers (in order to obtain better mechanical properties of the composite parts).

6.2. Shear locking angle

When a picture frame test is performed, wrinkles appear from a certain angle which has been called 'shear locking angle' [45,46,89,90]. This shear locking angle has been used as a limit beyond which a draping process leads to wrinkling. In particular, kinematic models (also called fishnet algorithms) rely on this locking angle to predict or not the onset of wrinkles (which are not described by these methods) [91-94]. It can be seen from the examples shown in Fig. 9 that the in-plane shear angles can reach very large values (70°), higher than the shear locking angle, without wrinkles occurring. This is possible thanks to the tensions induced in the textile reinforcement by the tools and the blank holder. The onset and development of wrinkles occur when the global equations of mechanics (Eq. 2 to 5) and the boundary conditions lead to an out-of-plane solution. This wrinkling phenomenon concerns all mechanical properties. In this paper it was proposed to take into account the in-plane shear and bending stiffnesses (because the

tensile stiffness is very large). Using the shear locking angle to rule on the occurrence of wrinkles means neglecting the bending stiffness which plays an important role in the occurrence and development of wrinkles. The forming processes analyzed in this article and in others show that it is necessary to take into account the bending stiffness.

6.3 Internal structure and weave pattern of the textile reinforcement

To achieve good drapability of a textile reinforcement, the shear stiffness must be low and the bending stiffness high. The internal geometry of the fabric plays a major role in determining the characteristics of a fabric that provide low shear stiffness and high bending stiffness. The weaving pattern is one element of fabric's internal geometry. Satin and interlock fabrics have good (low) Drapability Ratio. Plain Weave reinforcements, on the other hand, lead to more wrinkling. It is difficult to give a definitive rule on this point. On the other hand, it is quite easy, for a given textile reinforcement, to measure the in-plane shear and bending stiffness. The Drapability Ratio then gives a good indication of the drapability of the fabric.

In the case of biaxial NCFs, the stitch plays an important role with respect to stiffnesses and therefore drapability. The biaxial NCF studied in this paper shows a good drapability. The triaxial NCF and the isotropic sheet have an internal structure that does not allow them to be used in a draping process.

6.4. Consideration of in-plane shear and bending non-linearities

The determination of the Drapability Ratio presented above is based on constant values C_S and C_B of the stiffnesses of in-plane shear and bending. However, the in-plane shear and bending behaviors are generally non-linear (e.g. Fig. 4 for the in-plane shear of an interlock fabric). By considering constant values of C_S and C_B (which corresponds to linear behaviors), it is possible to calculate the Drapability Ratio which is a constant. But several choices for the determination of constants C_S and C_B can be considered. In in-plane shear, C_S is determined by the shear force for an angle of 40° . Different angles could be considered. The average of the stiffness for all the measured angles could also be used. In bending, Peirce's method assumes a linear behavior which allows to determine the constant C_B . But the bending behavior $M(\chi)$ is not linear in general [65, 68]. The mean stiffness over the interval $[0, \chi_{\max}]$ where χ_{\max} is the maximum measured curvature, can be an alternative to the bending stiffness given by Peirce method.

A study will be conducted to establish the optimal way to determine the C_S and C_B constants. It is nevertheless likely that the results will differ only slightly from those obtained by the approach proposed in Section 2. For example, a calculation of the Drapability Ratios was made using a shear angle of 30° (instead of 40° in the previous sections) and the corresponding shear force to determine C_S for all the reinforcements presented in this paper (Table 1). The Drapability Ratios were very slightly modified, and their relative order (Fig. 6 and 10) was not changed.

In this paper, the Drapability Ratio (DR) proposed to characterize the drapability of a textile reinforcement is a constant for the sake of simplicity. In order to differentiate between low and high curvature geometries, for each textile reinforcement, different DRs could be defined for forming leading to low shear angles by taking into account the shear stiffness for an angle of 20° (for example) and for forming requiring higher angles by taking into account the shear stiffness for an angle of 40° (as it was done in this paper). These two (or more) DR could be taken into account depending on the geometry of the part to be formed. This can be extended to the determination of a $DR(\gamma)$ curve for a given reinforcement.

7. Conclusion

The Drapability Ratio proposed in this paper is a simple evaluation of the drapability of a given textile composite reinforcement. It requires only the measurement (or estimation) of in-plane shear stiffness and bending stiffness. Wrinkle-free drape is favored by low shear stiffness and high bending stiffness. The Drapability Ratio is the ratio of these two stiffnesses and quantifies the drapability of the textile reinforcement.

A set of square box forming and cylinder forming tests showed the good correlation between the Drapability Ratio and wrinkling occurrence. The Drapability Ratio quantifies the drapability of a textile reinforcement, but it is not sufficient to predict a wrinkle-free draping for a given process. In addition to the drapability of the textile reinforcement, the parameters of the draping process such as the geometry of the tools and the blank holder forces are also essential. Nevertheless, the knowledge of the Drapability Ratio of a textile reinforcement is important to consider its use for draping on complex shapes. When a forming on a given shape has been done without wrinkling, all textile reinforcements with a lower Drapability Ratio will be able to be draped under the same conditions on this geometry. On the other hand, if a forming process leads to wrinkling, there is no point in trying to drape fabrics with a higher Drapability Ratio on this shape. The choice of an alternative textile reinforcement must be made among fabrics with a smaller Drapability Ratio.

It will be interesting to carry out studies to highlight the ways to control the Drapability Ratio of textile reinforcements. It appears that weaving patterns satin and interlock lead to lower Drapability Ratios than plain weave. The internal geometry of the weave of satins and interlocks leads to high bending stiffnesses while preserving a sufficiently low in-plane shear stiffness. When the reasons for these differences are well understood, it may be possible to manufacture reinforcements with a better drapability.

Acknowledgements

This work was supported by Agence Nationale de la Recherche, grant N° ANR-18-CE06-0011-04 AMOC and by the China Scholarship Council (CSC) (B. Chen).

References

- [1] Witten E, Mathes V. The Market for Glass Fibre Reinforced Plastics (GRP) in 2019: Market Developments, Trends Outlooks and Challenges; Industrievereinigung Verstärkte Kunststoffe e. V., Frankfurt am Main, Deutschland 2019.
- [2] Schmidt, T., May, D., Duhovic, M., Widera, A., Hümbert, M., & Mitschang, P. A combined experimental–numerical approach for permeability characterization of engineering textiles. *Polymer Composites* 2021;42(7), 3363-3379.
- [3] Ruiz E, Trochu F. 19 – Flow modeling in composite reinforcements. In: *Composite reinforcements for optimum performance*, Woodhead Publishing; 2011, p. 588–615.
- [4] Deléglise M, Le Grogne P, Binetruy C, Krawczak P, Claude B. Modeling of high speed RTM injection with highly reactive resin with on-line mixing. *Compos A Appl Sci Manuf* 2011;42:1390–7.
- [5] Sozer EM, Simacek P, Advani SG. 9 – Resin transfer molding (RTM) in polymer matrix composites. In: Advani SG, Hsiao K-T, editors. *Manufacturing techniques for polymer matrix composites (PMCs)*. Woodhead Publishing; 2012. p. 245–309
- [6] Sauer M. *Composites Market Report 2019—The Global CF- und CC-Market 2019: Market Developments, Trends, Outlook and Challenges*; Composites United e.V., Berlin, Deutschland 2019
- [7] Gereke T, Döbrich O, Hübner M, Cherif C. Experimental and computational composite textile reinforcement forming: A review. *Compos Part A Appl Sci Manuf* 2013;46:1–10.
- [8] Bussetta P, Correia N. Numerical forming of continuous fibre reinforced composite material: A review. *Compos Part A Appl Sci Manuf* 2018;113:12–31.
- [9] Liang B, Boisse P. A review of numerical analyses and experimental characterization methods for forming of textile reinforcements. *Chinese J Aeronaut* 2021;34:143–63.
- [10] Ten Thije RHW, Akkerman R, Huétink J. Large deformation simulation of anisotropic material using an updated Lagrangian finite element method. *Comput Methods Appl Mech Eng* 2007;196:3141–50.
- [11] Hamila N, Boisse P, Sabourin F, Brunet M. A semi - discrete shell finite element for textile composite reinforcement forming simulation. *Int J Numer Methods Eng* 2009;79:1443 – 66.
- [12] Jauffrès D, Sherwood JA, Morris CD, Chen J. Discrete mesoscopic modeling for the simulation of woven-fabric reinforcement forming. *Int J Mater Form* 2010;3:1205–16.
- [13] Haanappel SP, Ten Thije RHW, Sachs U, Rietman B, Akkerman R. Formability analyses of uni-directional and textile reinforced thermoplastics. *Compos Part A Appl Sci Manuf* 2014;56:80–92.
- [14] Daelemans L, Faes J, Allaoui S, Hivet G, Dierick M, Van Hoorebeke L, et al. Finite element simulation of the woven geometry and mechanical behaviour of a 3D woven dry fabric under tensile and shear loading using the digital element method. *Compos Sci Technol* 2016;137:177–87.
- [15] El Said B, Ivanov D, Long AC, Hallett SR. Multi-scale modelling of strongly heterogeneous 3D composite structures using spatial Voronoi tessellation. *J Mech Phys Solids* 2016;88:50–71.
- [16] Döbrich O, Gereke T, Cherif C. Modeling the mechanical properties of textile-reinforced composites with a near micro-scale approach. *Compos Struct* 2016;135:1–7.
- [17] Kärger L, Galkin S, Zimmerling C, Dörr D, Linden J, Oeckerath A, et al. Forming optimisation embedded in a CAE chain to assess and enhance the structural performance of composite components. *Compos Struct* 2018;192:143–52.
- [18] Yu F, Chen S, Viisainen J V, Sutcliffe MPF, Harper LT, Warrior NA. A macroscale finite element approach for simulating the bending behaviour of biaxial fabrics. *Compos Sci Technol* 2020;191:108078.
- [19] Bai R, Colmars J, Chen B, Naouar N, Boisse P. The fibrous shell approach for the simulation of composite draping with a relevant orientation of the normals. *Compos Struct* 2022:115202.
- [20] Allaoui S, Hivet G, Soulat D, Wendling A, Ouagne P, Chatel S. Experimental preforming of highly double curved shapes with a case corner using an interlock reinforcement. *Int J Mater Form* 2014;7:155–65.

- [21] Nezami FN, Gereke T, Cherif C. Analyses of interaction mechanisms during forming of multilayer carbon woven fabrics for composite applications. *Compos Part A Appl Sci Manuf* 2016;84:406–16.
- [22] Tephany C, Gillibert J, Ouagne P, Hivet G, Allaoui S, Soulat D. Development of an experimental bench to reproduce the tow buckling defect appearing during the complex shape forming of structural flax based woven composite reinforcements. *Compos Part A Appl Sci Manuf* 2016;81:22–33.
- [23] Boisse P, Hamila N, Madeo A. Modelling the development of defects during composite reinforcements and prepreg forming. *Philos Trans R Soc A Math Phys Eng Sci* 2016;374:20150269.
- [24] Lightfoot JS, Wisnom MR, Potter K. A new mechanism for the formation of ply wrinkles due to shear between plies. *Compos Part A Appl Sci Manuf* 2013;49:139–47.
- [25] Hallander P, Sjölander J, Åkermo M. Forming induced wrinkling of composite laminates with mixed ply material properties; an experimental study. *Compos Part A Appl Sci Manuf* 2015;78:234–45.
- [26] Boisse P, Hamila N, Vidal-Sallé E, Dumont F. Simulation of wrinkling during textile composite reinforcement forming. Influence of tensile, in-plane shear and bending stiffnesses. *Compos Sci Technol* 2011;71:683–92.
- [27] Döbrich O, Gereke T, Diestel O, Krzywinski S, Cherif C. Decoupling the bending behavior and the membrane properties of finite shell elements for a correct description of the mechanical behavior of textiles with a laminate formulation. *J Ind Text* 2014;44:70–84.
- [28] Dangora LM, Mitchell CJ, Sherwood JA. Predictive model for the detection of out-of-plane defects formed during textile-composite manufacture. *Compos Part A Appl Sci Manuf* 2015;78:102–12.
- [29] Thompson AJ, Belnoue JPH, Hallett SR. Modelling defect formation in textiles during the double diaphragm forming process. *Compos Part B Eng* 2020;202:108357.
- [30] Christ M, Miene A, Mörschel U. Measurement and analysis of drapeability effects of warp-knit NCF with a standardised, automated testing device. *Appl Compos Mater* 2017;24:803–20.
- [31] Chu CC, Cummings CL, Teixeira NA. Mechanics of elastic performance of textile materials: Part V: a study of the factors affecting the drape of fabrics—the development of a drape meter. *Text Res J* 1950;20:539–48.
- [32] Cusick GE. 46—The dependence of fabric drape on bending and shear stiffness. *J Text Inst Trans* 1965;56:T596–606.
- [33] Collier BJ. Measurement of fabric drape and its relation to fabric mechanical properties and subjective evaluation. *Cloth Text Res J* 1991;10:46–52.
- [34] Stylios GK, Powell NJ, Cheng L. An investigation into the engineering of the drapability of fabric. *Trans Inst Meas Control* 2002;24:33–50.
- [35] Lo WM, Hu JL, Li LK. Modeling a fabric drape profile. *Text Res J* 2002;72:454–63.
- [36] Lojen DZ, Jevsnik S. Some aspects of fabric drape. *Fibres Text East Eur* 2007;15:39.
- [37] Al-Gaadi B, Göktepe F, Halász M. A new method in fabric drape measurement and analysis of the drape formation process. *Text Res J* 2012;82:502–12.
- [38] Matusiak M. Influence of the structural parameters of woven fabrics on their drapeability. *Fibres Text East Eur* 2017.
- [39] Morooka H, Niwa M. Relation between drape coefficients and mechanical properties of fabrics. *J Text Mach Soc Japan* 1976;22:67–73.
- [40] Boisse P, Colmars J, Hamila N, Naouar N, Steer Q. Bending and wrinkling of composite fiber preforms and prepregs. A review and new developments in the draping simulations. *Compos Part B Eng* 2018;141:234–49.
- [41] Abdul Ghafour T, Colmars J, Boisse P. The importance of taking into account behavior irreversibilities when simulating the forming of textile composite reinforcements. *Compos Part A Appl Sci Manuf* 2019;127:105641.
- [42] Danckert J. Experimental investigation of a square-cup deep-drawing process. *J Mater Process Technol* 1995;50:375–84.
- [43] Yoon JW, Yang DY, Chung K, Barlat F. A general elasto-plastic finite element formulation based on incremental deformation theory for planar anisotropy and its application to sheet metal forming. *Int J Plast* 1999;15:35–67.

- [44] Potter K. Bias extension measurements on cross-plyed unidirectional prepreg. *Compos Part A Appl Sci Manuf* 2002;33:63–73.
- [45] Lebrun G, Bureau MN, Denault J. Evaluation of bias-extension and picture-frame test methods for the measurement of intraply shear properties of PP/glass commingled fabrics. *Compos Struct* 2003;61:341–52.
- [46] Sharma SB, Sutcliffe MPF, Chang SH. Characterisation of material properties for draping of dry woven composite material. *Compos A Appl Sci Manuf* 2003;34:1167–75.
- [47] Lomov SV, Verpoest I. Model of shear of woven fabric and parametric description of shear resistance of glass woven reinforcements. *Compos Sci Technol* 2006;66:919–33.
- [48] Cao J, Akkerman R, Boisse P, Chen J, Cheng HS, de Graaf EF, et al. Characterization of mechanical behavior of woven fabrics: experimental methods and benchmark results. *Compos A Appl Sci Manuf* 2008;39:1037–53.
- [49] Zhu B, Yu TX, Teng J, Tao XM. Theoretical modeling of large shear deformation and wrinkling of plain woven composite. *J Compos Mater* 2009;43:125–38.
- [50] Boisse P, Hamila N, Guzman-Maldonado E, Madeo A, Hivet G, dell'Isola F. The bias-extension test for the analysis of in-plane shear properties of textile composite reinforcements and prepregs: a review. *Int J Mater Form* 2017;10:473–92.
- [51] Hosseini A, Kashani MH, Sassani F, Milani AS, Ko FK. Identifying the distinct shear wrinkling behavior of woven composite preforms under bias extension and picture frame tests. *Compos Struct* 2018;185:764–73.
- [52] Boisse P, Cherouat A, Gelin JC, Sabhi H. Experimental study and finite element simulation of a glass fiber fabric shaping process. *Polym Compos* 1995;16:83–95.
- [53] Cherouat A, Billoet JL. Mechanical and numerical modelling of composite manufacturing processes deep-drawing and laying-up of thin pre-impregnated woven fabrics. *J Mater Process Technol* 2001;118:460–71.
- [54] Cao J, Xue P, Peng X, Krishnan N. An approach in modeling the temperature effect in thermo-stamping of woven composites. *Compos Struct* 2003;61:413–20.
- [55] Yu WR, Zampaloni M, Pourboghra F, Chung K, Kang TJ. Analysis of flexible bending behavior of woven preform using non-orthogonal constitutive equation. *Compos Part A Appl Sci Manuf* 2005;36:839–50.
- [56] Skordos AA, Monroy Aceves C, Sutcliffe MPF. A simplified rate dependent model of forming and wrinkling of pre-impregnated woven composites. *Compos Part A Appl Sci Manuf* 2007;38:1318–30.
- [57] Lin H, Wang J, Long AC, Clifford MJ, Harrison P. Predictive modelling for optimization of textile composite forming. *Compos Sci Technol* 2007;67:3242–52.
- [58] Chen S, Harper LT, Endruweit A, Warrior NA. Formability optimisation of fabric preforms by controlling material draw-in through in-plane constraints. *Compos Part A Appl Sci Manuf* 2015;76:10–9.
- [59] Boisse P, Hamila N, Vidal-Salle E, Dumont F. Simulation of wrinkling during textile composite reinforcement forming. Influence of tensile, in-plane shear and bending stiffnesses. *Compos Sci Technol* 2011;71:683–92.
- [60] Dangora LM, Mitchell CJ, Sherwood JA. Predictive model for the detection of out of-plane defects formed during textile-composite manufacture. *Compos Part A Appl Sci Manuf* 2015;78:102–12.
- [61] Thompson AJ, Belnoue JP-H, Hallett SR. Modelling defect formation in textiles during the double diaphragm forming process. *Compos Part B Eng* 2020;202: 108357.
- [62] Huang J, Boisse P, Hamila N, Gnaba I, Soulat D, Wang P. Experimental and numerical analysis of textile composite draping on a square box. Influence of the weave pattern. *Compos Struct* 2021;267:113844.
- [63] Wang P, Legrand X, Boisse P, Hamila N, Soulat D. Experimental and numerical analyses of manufacturing process of a composite square box part: comparison between textile reinforcement forming and surface 3D weaving. *Compos B Eng*, 2015;78:26–34.
- [64] Lomov S V, Boisse P, Deluycker E, Morestin F, Vanclooster K, Vandepitte D, et al. Full-field strain measurements in textile deformability studies. *Compos Part A Appl Sci Manuf* 2008;39:1232–44.

- [65] Wang J, Page JR, Paton R. Experimental investigation of the draping properties of reinforcement fabrics. *Compos Sci Technol* 1998; 58:229–237
- [66] Harrison P, Clifford MJ, Long AC. Shear characterisation of viscous woven textile composites, a comparison between picture frame and bias-extension experiments. *Compos Sci Technol* 2004; 64: 1453–1465
- [67] Peng XQ, Cao J. A continuum mechanics-based non-orthogonal constitutive model for woven composite fabrics. *Compos Part A Appl Sci Manuf* 2005;36:859–74.
- [68] Syerko E, Comas-Cardona S, Binetruy C. Models for shear properties/behavior of dry fibrous materials at various scales: a review. *Int J Mater Form* 2015;8:1–23.
- [69] Launay J, Hivet G, Duong AV, Boisse P. Experimental analysis of the influence of tensions on in plane shear behaviour of woven composite reinforcements. *Compos Sci Technol* 2008; 68:506–515
- [70] Kawabata S. The standardization and analysis of hand evaluation. Osaka: The Textile Machinery Society of Japan; 1980.
- [71] Lomov S V, Verpoest I, Barburski M, Laperre J. Carbon composites based on multiaxial multiply stitched preforms. Part 2. KES-F characterisation of the deformability of the preforms at low loads. *Compos Part A Appl Sci Manuf* 2003;34:359–70.
- [72] Sachs U, Akkerman R. Viscoelastic bending model for continuous fiber-reinforced thermoplastic composites in melt. *Compos A Appl Sci Manuf* 2017;100:333–41.
- [73] Peirce FT. The “handle” of cloth as a measurable quantity. *J Textil Inst Trans* 1930;21(9):T377–416.
- [74] ASTM. Standard test method for stiffness of fabrics, chap. D1388–D1396(2002). Philadelphia: American Society for Testing and Materials; 2002
- [75] De Bilbao E, Soulat D, Hivet G, Gasser A. Experimental Study of Bending Behaviour of Reinforcements. *Exp Mech* 2010;50:333–51.
- [76] Syerko E, Comas-Cardona S, Binetruy C. Models of mechanical properties/behavior of dry fibrous materials at various scales in bending and tension: A review. *Compos Part A Appl Sci Manuf* 2012;43:1365–88.
- [77] Lammens N, Kersemans M, Luyckx G, Van Paepegem W, Degrieck J. Improved accuracy in the determination of flexural rigidity of textile fabrics by the Peirce cantilever test (ASTM D1388). *Textile Res J* 2014;84(12):1307–14.
- [78] Liang B, Chaudet P, Boisse P. Curvature determination in the bending test of continuous fibre reinforcements. *Strain* 2017;53:e12213.
- [79] Peng X, Ding F. Validation of a non-orthogonal constitutive model for woven composite fabrics via hemispherical stamping simulation. *Compos A Appl Sci Manuf* 2011;42:400–7
- [80] Nishi M, Taketa I, Iwata A, Hirashima T. Constitutive modeling of carbon fiber fabric: from material parameter identification to application in FE forming simulation. 17th European conference on composite materials; 2016
- [81] Bae D, Kim S, Lee W, Yi JW, Um MK, Seong DG. Experimental and numerical studies on fiber deformation and formability in thermoforming process using a fast-cure carbon prepreg: effect of stacking sequence and mold geometry. *Materials* 2018;11:857
- [82] Chen B, Colmars J, Naouar N, Boisse P. A hypoelastic stress resultant shell approach for simulations of textile composite reinforcement forming. *Compos Part A Appl Sci Manuf* 2021;149:106558.
- [83] Dörr D, Schirmaier FJ, Henning F, Kärger L. A viscoelastic approach for modeling bending behavior in finite element forming simulation of continuously fiber reinforced composites. *Compos Part A Appl Sci Manuf* 2017;94:113–23.
- [84] Duhovic M, Bhattacharyya D. Simulating the deformation mechanisms of knitted fabric composites. *Compos Part A Appl Sci Manuf* 2006;37:1897–915.
- [85] Dusserre G, Balea L, Bernhart G. Elastic properties prediction of a knitted composite with inlaid yarns subjected to stretching: A coupled semi-analytical model. *Compos Part A Appl Sci Manuf* 2014;64:185–93.
- [86] Azzam, H. A. Compressive properties of stretch-broken carbon fibre (SBCF)/polyamide 12 commingled unidirectional composites. *Autex Research Journal* 2007, 7(3), 166-179.

- [87] Taketa I, Sato N, Kitano A, Nishikawa M, Okabe T. Enhancement of strength and uniformity in unidirectionally arrayed chopped strands with angled slits. *Compos Part A Appl Sci Manuf* 2010;41:1639–46.
- [88] Wang P, Hamila N, Boisse P, Chaudet P, Lesueur D. Thermo-mechanical behavior of stretch-broken carbon fiber and thermoplastic resin composites during manufacturing. *Polym Compos* 2015;36:694–703.
- [89] Prodromou AG, Chen J. On the relationship between shear angle and wrinkling of textile composite preforms. *Compos Part A Appl Sci Manuf* 1997;28:491–503.
- [90] Rozant O, Bourban P-E, Månson J-A. Drapability of dry textile fabrics for stampable thermoplastic preforms. *Compos Part A Appl Sci Manuf* 2000;31:1167–77.
- [91] Van Der Ween F. Algorithms for draping fabrics on doubly curved surfaces. *Int J Numer Meth Eng* 1991;31:1414–26
- [92] Long A C, Rudd C D. A simulation of reinforcement deformation during the production of preform for liquid moulding processes, I. *Mech. E. J. Eng. Manuf.* 1994; 208, 269-278.
- [93] Potluri P, Sharma S, Ramgulam R. Comprehensive drape modelling for moulding 3D textile preforms. *Compos Part A Appl Sci Manuf* 2001;32:1415–24.
- [94] Hancock SG, Potter KD. The use of kinematic drape modelling to inform the hand lay-up of complex composite components using woven reinforcements. *Compos Part A Appl Sci Manuf* 2006;37:413–22.